RSC Advances

ROYAL SOCIETY OF CHEMISTRY

www.rsc.org/advances

Facile hydrothermal synthesis of a highly efficient solar active Pr_6O_{11}-ZnO Photocatalyst and its multiple applications

Subramanian Balachandran, Kuppulingam Thirumalai and Meenakshisundaram Swaminathan*

Department of Chemistry, Annamalai University, Annamalainagar 608 002, India.

*Corresponding author: Address

Dr. M. Swaminathan
Emeritus Professor
Department of Chemistry
Annamalai University
Annamalainagar 608 002
Tel/Fax: +91 4144 225072
E-mail: chemres50@gmail.com

Coupled semiconductor oxide nanomaterial Pr_6O_{11}-ZnO was fabricated by a simple hydrothermal method and characterized by X-ray diffraction (XRD), field emission scanning electron microscopy (FE-SEM), elemental color mapping, high resolution transmission electron microscopy (HR-TEM), X-ray photoelectron spectroscopy (XPS) , UV-Vis diffuse reflectance spectroscopy (DRS), photoluminescence spectroscopy and BET surface area measurements. XRD analysis reveals that the as synthesized product has face-centered cubic phase of Pr_6O_{11} and hexagonal wurtzite phase of ZnO. FE-SEM images of Pr_6O_{11}-ZnO show the nanochain like structures and Pr_6O_{11} nanoparticles were homogeneously dispersed on the ZnO surface. The XPS analysis shows the presence of Zn, O and Pr elements and their oxidation states. Pr_6O_{11}-ZnO has increased absorption in the UV as well as visible region. The photocatalytic activity toward degradation of Acid Violet 7 (AV 7) under natural sunlight was investigated. Pr_6O_{11}-ZnO exhibits higher photocatalytic activity when compared to pure ZnO and Pr_6O_{11} particles. Pr_6O_{11}-ZnO is more advantageous in toxic azodye degradation because of its reusability and higher efficiency at the neutral pH 7. Hydrophobicity of Pr_6O_{11}-ZnO has been evaluated using contact angle measurements. Pr_6O_{11}-ZnO modified TEOS coated glass subtracts shows a significant hydrophobic property. Pr_6O_{11}-ZnO exhibits high DC and photoconductivity, which make it useful for soliton wave communication and solar cell applications. Our results provide some new insights on the performance of a solar active photocatalysts, self cleaning and highly conductive materials.

1. Introduction

In the last two decades, energy shortage and environmental deterioration have become the major obstacles to the development of economy and society. Semiconductor photocatalysts have attracted much attention, owing to their applications to environmental purification and solar energy conversion. Many semiconductors oxides, such as TiO_2, ZnO, WO_3, Nb_2O_5 and Bi_2O_3, have been employed as photocatalysts in toxic organic pollutant degradation and water splitting reactions.[1-5]

Zinc Oxide as an important wide and direct band-gap semiconductor (3.2 eV) is a promising photocatalyst because of its high catalytic efficiency, low cost, and environmental sustainability. It is also one of the most promising materials for optoelectronic applications due to its wide band gap and large exciton binding energy of 60 meV. The ZnO materials with highly controlled structures and uniform morphologies generally have novel physical and chemical properties. Nevertheless, the large band gap of ZnO (3.2 eV) limits its use under UV light, which constitutes only 5% of the total solar spectrum. There are many rare earth metals such as Pr,[6] Sm,[7] Nd,[8] Ce, Y,[9] and Eu,[10] that have been utilized to promote the separation of photogenerated electron and hole for improving photocatalytic property. The oxides of rare earth elements have been extensively used in past decades due to their optic, electric, magnetic, and catalytic properties. Some of the rare earth oxides Dy_2O_3,[11] Eu_2O_3,[12] La_2O_3,[13] and CeO_2,[14-17] with high thermal stability have been synthesized by various methods and used for catalytic and photocatalytic applications. Praseodymium oxides have a special position within the series of the rare-earth oxides. The oxides of praseodymium represent a system of phases having Pr_2O_3 and PrO_2, Pr_6O_{11} and five suboxides, whose composition is variable with defective structure.[18,19] Among the different phases, Pr_6O_{11} is the stable one at room temperature and its morphological

and structural characteristics of have been reported.[18] From the XRD pattern of Pr_6O_{11}, the presence of both Pr^{4+} and Pr^{3+} cations in the lattice was established.[20] It has the highest oxygen ion mobility in the series of lanthanide oxides, because of the fast changes in the oxidation states of praseodymium.[21] Praseodymium oxides are used as catalysts, catalyst carriers, promoters, stabilizers and higher electrical conductive materials.[22,23] Photopyroelectric characteristics of Pr_6O_{11}-ZnO-ceramic composites and anticorrosion applications of modified silane coatings with Pr_6O_{11}-ZnO were analysed.[24,25]

In the field of photocatalysts, one of the effective ways to enhance the electron-hole separation is to use coupled semiconductor oxides. Coupling of ZnO with Pr_6O_{11} having high oxygen ion mobility and variable valency is expected to have an efficient system for catalytic and other applications. In continuation of earlier work on modified ZnO,[26, 27] we present here the fabrication of coupled oxide Pr_6O_{11}-ZnO and its multiple applications. The photocatalytic activity of coupled Pr_6O_{11}-ZnO has been tested by the degradation of an azodye AV 7 under solar light irradiation.

Self cleaning is one of the promising applications in industrial engineering and it is determined by contact angle measurements. Contact angle quantifies the wettability of a solid surface by a liquid via the Young equation. Hydrophobicity is a property that provides water repellency and non-wettability of a solid surface.[28,29] Leaves of some plants, notably the Lotus leaves, exhibit this property as an essential part of a self-cleaning mechanism. Heterostructured nanocomposites show good hydrophobicity. We tested the hydrophobicity and conductivity of Pr_6O_{11}-ZnO. We believe that our findings can open a new and effective avenue to further improve the solar photocatalytic activity, self cleaning and conductivity applications of coupled systems.

Experimental Section

2.1. Materials.

Praseodymium oxide, Analar grade Zinc nitrate hexahydrate, Oxalic acid dihydrate, and Ethanol were obtained from Himedia chemicals and used as such. Acid Violet 7 (Fig.S1) from Colour Chem, Pondicherry and ZnO (Merck chemicals, surface area $5m^2\ g^{-1}$, particle size 4.80 μm) were used as received. A gift sample of TiO_2-P25 (80% anatase, 20% rutile with BET surface area 50 $m^2\ g^{-1}$ and mean particle size of 30 nm) was supplied by Evonik, Germany. Deionized distilled water was employed in all experiments.

2.2.1. Preparation of Pr_6O_{11}-ZnO.

11.90 g of $Zn(NO_3)_2.6H_2O$ (0.4 M) was dissolved in 100 mL deionized distilled water under stirring to form a clear solution A and then 0.243 g of Pr_6O_{11} was dispersed in Solution A to get a dark brown color suspension. 100 ml aqueous solution of Oxalic acid (0.6 M) was introduced into suspension drop wise and stirred for 4 h to ensure complete precipitation of Zinc oxalate dihydrate. Then the mixture was transferred into a Teflon lined stainless steel autoclave, sealed and heated at 120 °C for 48 h. Precipitated Zinc oxalate dihydrate along with Praseodymium hydroxide was filtered, washed with distilled water and ethanol, and dried in air at 90 °C for 12 h. Precipitate was calcined at 450 °C for 4 h in a muffle furnace to get Pr_6O_{11}-ZnO. It is found that this catalyst contained 9 wt% Pr_6O_{11}. Catalysts with 3wt%, 6wt% and 12wt% of Pr_6O_{11} were prepared by addition of appropriate amounts Pr_6O_{11} using the same method. It is found that the AV 7 degradation efficiency of 3, 6, 9 and 12 wt% Pr_6O_{11} on ZnO are 91, 94.6, 98.2 and 96 % respectively. Hence the catalyst with 9 wt% Pr_6O_{11} was characterized using various techniques.

2.2. Characterization

Thermogravimetric analysis was carried out using TGA Q50 TA instruments. X-ray diffraction (XRD) patterns were recorded with a Siemens D5005 diffractometer using Cu Kα (k = 0.151 418 nm) radiation. Maximum peak positions were compared with the standard files to identity the crystalline phase. The surface morphology of the Pr_6O_{11}-ZnO was studied by using a field emission scanning electron microscope (FE-SEM) (Model ULTRA-55). EDS analysis was performed on gold coated samples using a FE-SEM (Model ULTRA-55). X-Ray photoelectron spectra (XPS) of the catalysts were recorded in an ESCA-3 Mark II spectrometer (VG Scientific Ltd., England) using Al Kα (1486.6 eV) radiation as the source. The spectra were referenced to the binding energy of C (1s) (285 eV). Diffuse reflectance spectra were recorded with Shimadzu UV-2450. UV absorbance measurements were taken using Hitachi-U-2001 spectrometer. The specific surface areas of the samples were determined through nitrogen adsorption at 77 K on the basis of the BET equation using a Micrometrics ASAP 2020 V3.00 H. A sample mass of about 30 mg was used for adsorption analysis after pretreatment at 393 K under vacuum conditions and kept in N_2 atmosphere until N_2-adsorption measurements. The water contact angles were measured using a Drop Shape Analyzer (DSA) (Kru¨ss GmbH, Germany).

The Scherrer formula (equation 1) was employed for the calculation of the average crystallite size of Pr_6O_{11}-ZnO.

$$\Phi = \frac{K\lambda}{\beta \cos\theta} \qquad \text{---------- (1)}$$

Where Φ is the crystallite size, λ is the wavelength of X-ray used; *K* is the shape factor, β is the full line width at the half-maximum height of the peak, and θ is the Bragg angle. Particles sizes were calculated using all the intense peaks. The average particle size of Pr_6O_{11}-ZnO is 6.4 nm.

2.3. Photocatalytic degradation

All photocatalytic experiments were carried out under similar conditions on sunny days of April-May 2012 between 11 am and 2 pm. An open borosilicate glass tube of 50 mL capacity, 40 cm height and 20 mm diameter was used as the reaction vessel. The suspensions were magnetically stirred in the dark for 30 min to attain adsorption-desorption equilibrium between the dye and Pr_6O_{11}-ZnO. Irradiation was carried out in the open air condition. 50 mL of dye solution with Pr_6O_{11}-ZnO was continuously aerated by a pump to provide oxygen and for the complete mixing of reaction solution. During the illumination time no volatility of the solvent was observed. After dark adsorption the first sample was taken. At specific time intervals, 2 mL of the sample was withdrawn and centrifuged to separate the catalyst. 1 mL of the centrifugate was diluted to 10 mL and its absorbance was measured at 306 nm for AV 7 dye. The absorbance at 306 nm represents the aromatic content of AV 7 and its decrease indicates the degradation of dye.

Solar light intensity was measured for every 30 min and the average light intensity over the duration of each experiment was calculated. The sensor was always set in the position of maximum intensity. The intensity of solar light was measured using LT Lutron LX-10/A Digital Lux meter and the intensity was 1250x100 ± 100 lux. The intensity was nearly constant during the experiments.

2.4. Contact angle and conductivity measurements

Coatings with catalysts and tetra ethoxysilane (TEOS) were successfully fabricated on a glass substrates using spin coating method at room temperature. Catalysts coated substrates were sintered at 125 °C for 3 h with heating rate of 5 °C/min in programmed furnace to ensure

densification of the gel network. A water droplet of 4µl was placed on the coating and its water contact angle was measured. The average of 5 measurements is reported as the water contact angle (WCA) on the substrate.

DC conductivity of the catalyst was taken using 6517B Keithley high resistance electrometer at room temperature. To make proper electrical contact, the samples were pasted with silver plates on both sides and sandwitched between two copper electrodes.

3. Results and discussions

3.1. Phase Structures and Morphology.

The thermal characteristics of synthesized Zinc Oxalate and mixed precipitate of praseodymium oxide-zinc oxalate precursors have been analyzed. In zinc oxalate (Fig. 1a) first weight loss occurred at 145 °C, which corresponds to the conversion of zinc oxalate dihydrate to anhydrous zinc oxalate due to the loss of two water molecules. The second weight loss at 410 °C, is attributed to the decomposition of anhydrous zinc oxalate to zinc oxide. In the case of mixture of praseodymium oxide-zinc oxalate, first weight loss occurred at 163 °C and the second weight loss was obtained around 445 °C. Thermogravimetric curve of mixed precipitate of praseodymium oxide-zinc oxalate (Fig. 1b) is similar to that of zinc oxalate (Fig. 1a) except an increase in decomposition temperature. This shows that in both cases only the conversion of zinc oxalate dihydrate to zinc oxide takes place. As there is no additional weight loss in mixed precipitate of praseodymium oxide-zinc oxalate, it is confirmed that there is no decomposition of praseodymium oxide in the mixed precipitate and thermal stability of the catalyst is also increased when compared to zinc oxalate.

XRD patterns of the prepared ZnO, Praseodymium hydroxide along with zinc oxalate (before calcination) and 9 wt% Pr_6O_{11}-ZnO are shown in fig. 2a-c respectively. The diffraction peaks of ZnO at 31.77, 34.49, 36.24, 56.60, 62.85, 66.38, 67.94, 69.08, 72.50 and 76.93° correspond to (1 0 0), (0 0 2), (1 0 1), (1 1 0), (1 0 3), (2 2 0), (1 1 2), (2 0 1), (0 0 4) and (2 0 2) planes of wurtzite ZnO (Fig. 2a).[30] In Fig.2b the diffraction peaks can be indexed to a hexagonal structure of $Pr(OH)_3$ (Joint Committee on Powder Diffraction Standards (JCPDS) Card No. 83-2304). The diffraction peaks (1 1 1), (2 0 0), (2 2 0), (3 1 1), (2 2 2), (4 0 0), (3 3 1), and (4 2 0) in fig. 2c are due to Pr_6O_{11} phase with a face-centered cubic structure (JCPDS Card No. 42-1121). The Pr_6O_{11} phase is more stable than the PrO_2 phase at ambient temperature in air.[31] All peaks of Pr_6O_{11} and ZnO absolutely matched with Pr_6O_{11}-ZnO (Fig.2c). X-ray diffractograms of Pr_6O_{11}-ZnO with different percentages of Pr_6O_{11} (3wt%, 6wt%, 9wt% and 12wt %) in ZnO are shown in Fig.S2. The diffraction peaks of Pr_6O_{11} increase with increase in its percentage. Therefore, it is clear from the XRD patterns that the nanocomposites have Pr_6O_{11} and ZnO as the face-centered cubic and the wurtzite phases, which is unique to our synthesized material.

The morphology of the catalyst was studied using a field emission scanning electron microscope. Fig. 3 shows the FE-SEM images of the Pr_6O_{11}-ZnO composite. Our sample showed a porous structure agglomerated with very small particles. It can be clearly seen that the catalyst basically look like a nanochain with the size ranging from 12 to 20 nm (Fig. 3a), which is mainly assembled by nanoparticles. It appears like a step formation (Fig. 3c). It may be due to the nano particles in nanochain like structures. The nanochain is made up of ZnO and nanoparticles of Pr_6O_{11} are dispersed on the surface of ZnO. Formation of ZnO nanochain has been reported earlier.[32] The nanochains are joined together to form a rock like structure (Fig.3b, 3c).

To confirm the distribution of Zn, O and Pr in the surface of the catalyst, elemental mapping of FE-SEM was carried out. Fig. 4 (a) exhibits FE-SEM color image of Pr_6O_{11}–ZnO, while figs. 4 b, c and d show the elemental mapping for Zinc, Oxygen and Praseodymium respectively. It is evident from the fig. 4 b and c that Zn and O are higher in density. There is a homogenous distribution of Zn, O and Pr (Fig. 4a). Thus elemental mapping shows that the catalyst is composed of Zn, O and Pr. This also indicates the purity of the catalyst Pr_6O_{11}–ZnO. The EDS recorded from the selected area is shown in fig. S3, which reveals the presence of Zn, O and Pr in the catalyst.

The HR-TEM analysis provides more information of the structure of 9wt% Pr_6O_{11}-ZnO. Fig. 5a and 5c show the images of particles of Pr_6O_{11}-ZnO at different locations and Fig.5b and 5d show the lattice fringes of Fig. 5a and 5c. Self nucleated and isolated Pr_6O_{11} or ZnO are not observed, indicating the formation of a Pr_6O_{11}-ZnO heterojunction. As seen in Fig. 5a and 5c the sizes of the particles are less than 10 nm showing their existence as quantum dots. This is also confirmed by particle size distribution of 1 to 10 nm shown in fig. 5f. The HRTEM images (Fig.5b and 5d) show a distinguished interface and the continuity of lattice fringes between the Pr_6O_{11} and ZnO, confirming the formation of chemical bonds between them. They also show the uniform lattice structure of the hexagonal wurtzite ZnO. The spacing between adjacent lattice fringes is 0.256 nm, which is close to the d spacing of the (002) plane of ZnO. The interference fringe spacing of the individual praseodymium oxide is approximately 0.32 nm, being consistent with the inter planar distance of the (111) plane in the face-centered cubic structure of Pr_6O_{11}.[31] Fig.5e shows the selected area electron diffraction (SAED) pattern of the catalyst. Fig. 5 (f) shows an average particle size histogram of Pr_6O_{11}–ZnO. From this histogram, average particle size of Pr_6O_{11}–ZnO is found to be 9.3 nm.

In order to determine the valance states of the various elements in Pr_6O_{11}-ZnO, XPS study was carried out. The survey spectra of Pr_6O_{11}-ZnO confirmed the presence of Pr, O and Zn. The binding energies (BEs) were calibrated using the C 1s energy of 284.6 eV. As shown in Fig.6a single C 1s peak is attributed to adventitious carbon that seems to exhibit an unavoidable presence on all air exposed materials. In Fig. 6b, the O 1s profile is asymmetric and can be fitted to two symmetrical peaks (α and β locating at 530.8 and 532.8 eV, respectively), indicating two different kinds of O species in the sample. The O1s peak at 532.8 eV is usually attributed to the presence of loosely bound oxygen on the surface of ZnO. The low binding energy component located at 530.8 eV is attributed to the O^{2-} ions in wurtzite structure of a hexagonal Zn^{2+} ion in Pr_6O_{11}-ZnO and the intensity of this peak is connected to the variations in the concentration of oxygen vacancies.[33] Therefore, changes in the intensity of this component may be connected in part to the variations in the concentration of oxygen vacancies. We can find that the peak at 530.8 eV is stronger in the catalyst. Two symmetric peaks at 1021.9 and 1045.1 eV in the high resolution XPS spectrum of Zn 2p are assigned to Zn $2p_{3/2}$ and Zn $2p_{1/2}$, indicating the existence of Zn^{2+} in the Pr_6O_{11}-ZnO (Fig. 6c).[34] Two symmetric peaks at 953.5 and 933.9 eV, which represent the $3d_{3/2}$ and $3d_{5/2}$ electrons of Pr, respectively (Fig. 6d). As reported earlier the peaks at 953.6 and 933.2 are due to the existence of Pr(3+) and Pr(4+) ions in Pr_6O_{11}[18, 34, 35]. The slight upword shift may be due to the interaction of ZnO in the lattice.

To determine the optical properties, UV-vis diffuse reflectance and photoluminescence spectra for the ZnO and Pr_6O_{11}-ZnO catalysts were recorded. Pr_6O_{11}-ZnO shows an increased absorption over the undoped ZnO material both in the visible and the ultraviolet regions (Fig.7). UV-Vis spectra in the diffuse reflectance mode (R) were transformed to the Kubelka-Munk function F(R) to separate the extent of light absorption from scattering. The band gap energy was

obtained from the plot of the modified Kubelka-Munk function $(F(R)E)^{1/2}$ versus the energy of the absorbed light E (equation 2)

$$F(R)E^{1/2} = \left[\frac{(1-R)^2}{2R} \times h\nu\right]^{1/2} \quad \text{(2)}$$

Band gap energies for ZnO, Pr_6O_{11} and Pr_6O_{11}-ZnO are 3.2, 2.69, 3.11 eV respectively (**Fig. S4**). Any impurity in the semiconductor oxide can form intermittent band energy levels and this leads to the decrease of bandgap energy, which increases the UV-visible absorption. Reduction of bandgap energy by the addition of Pr_6O_{11} has been reported earlier.[24] The photoluminescence (PL) can be used to find out the fate of electron–hole pairs in semiconductor particles. The PL emission results from the recombination of photoinduced charge carriers and a strong correlation between PL intensity and photocatalytic activity has been previously reported.[36] Fig. 8 presents the photoluminescence spectra of the prepared ZnO (a), and Pr_6O_{11}-ZnO (b). The emission band at 418 nm (2.92 eV) corresponds to the electron-hole recombination of ZnO.[37–40] Reduction of PL intensity at 418 nm by Pr_6O_{11}-ZnO when compared to prepared ZnO indicate the suppression of recombination of the photogenerated electron–hole pair. This suppression is caused by the electron capture by loaded Pr_6O_{11} on ZnO.

The pore structure of Pr_6O_{11}−ZnO composite sample was investigated by nitrogen adsorption−desorption isotherms, and the pore size distribution was calculated by Barrett–Joyner–Halenda (BJH) method. The N_2 adsorption/desorption isotherms of the synthesized Pr_6O_{11}−ZnO sample shown in fig. 9 exhibit a type III isotherm with a H3 hysteresis loop according to the classification of IUPAC.[41] A sharp increase in adsorption volume of N_2 is observed and located in the P/P_0 range of 0.80 to 0.99. This sharp increase can be attributed to the capillary condensation, indicating the good homogeneity of the sample and mesoporous size

because the P/P_0 position of the inflection point is related to the pore. Average pore radius of Pr_6O_{11}−ZnO, shown by pore size distribution curve in the inset of fig. 9, is 200 Å. The pore size distribution of the Pr_6O_{11}−ZnO sample thus confirms the mesoporous structure. Surface area measurements, determined by the BJH method, provide the specific surface area of Pr_6O_{11}−ZnO as 28.86 $m^2 g^{-1}$, which is higher than the prepared ZnO (11.52 $m^2 g^{-1}$) and Pr_6O_{11} (14.96 $m^2 g^{-1}$).

3.2. Photocatalytic Activity

Dye factories across the world are dumping millions of tons of dye effluent into rivers. The azo dyes are known to be dangerous and carcinogenic. The photocatalytic activity of the Pr_6O_{11}-ZnO samples was evaluated and compared with ZnO, Pr_6O_{11} by the degradation of an azo dye AV 7 (Fig. 10) under natural sun light irradiation. Fig. 10 shows the percentage of AV 7 degradation under different conditions with solar light. It is observed that almost complete degradation (99.4%) of AV 7 takes place at the time of 75 min with Pr_6O_{11}−ZnO under solar light. About 40.1% decrease in dye concentration occurred at pH 7 for the same experiment performed in the absence of solar light and this might be due to the adsorption of the dye on the surface of the catalyst. Dye resists self-photolysis. These observations reveal that both solar light and Pr_6O_{11}−ZnO are needed for effective destruction of AV 7. When prepared ZnO, Pr_6O_{11} and TiO_2-P25 were used under same conditions only 86.2, 82 and 75.3% degradations occurred, respectively. Pr_6O_{11}-ZnO showed higher photocatalytic activity than pure ZnO, due to higher charge separation. In the absence of light irradiation, 40% of AV 7 dye removal was observed because of the adsorption of dye molecules on the Pr_6O_{11}−ZnO surface. This higher adsorption may be due to increased surface area. UV spectral changes of AV 7 at different irradiation times with Pr_6O_{11}-ZnO catalyst are shown in Fig. S5. There is a gradual decrease in intensity without the

appearance of new absorption peaks. This reveals that the intermediates formed during degradation do not absorb at the analytical wavelength.

The percentage of degradation in the solar process is affected by variables such as pH and catalyst loading. Percentages of solar degradation at different pH from 3-11 for AV 7 are shown in Fig. S6. It is observed that the degradation rate increases with a raise in pH up to 7 and then decreases. After 75 min of irradiation, the percentages of AV 7 degradation are 40, 84, 99.4, 45, and 30 at pH 3, 5, 7, 9, and 11, respectively. Hence the optimum pH for efficient AV 7 removal on Pr_6O_{11}−ZnO is 7. To find out the reason for the effect of pH on degradation efficiency, zero point charge (ZPC) of the catalyst was determined by the potentiometric titration method.[42] Zero point charge of Pr_6O_{11}−ZnO was found to be 7.2, which is less than ZPC of ZnO (8.7). When the pH is above ZPC, the surface charge density of the catalyst becomes negative. This affects the adsorption of dye molecules, which exist anionic at pH above 7. Hence the degradation efficiency is low at pH 9 and 11. Low removal efficiency at the acidic pH range may be due to the dissolution of ZnO in Pr_6O_{11}−ZnO. Pr_6O_{11}−ZnO is more advantageous than ZnO and Pr_6O_{11} in the degradation of AV 7 because it has maximum efficiency at the neutral pH 7.

The influence of the photocatalyst quantity on the degradation of AV 7 has been investigated by employing different concentrations of Pr_6O_{11}−ZnO.The results are presented in Fig. S7. AV 7 dye degradation increases up to 4 g/L and a further increase of the catalyst quantity decreases the removal rate. The improvement of the removal rate is caused by i) the increase in the amount of catalyst weight which increases the number of dye molecules adsorbed and ii) the increase in the density of particles in the area of illumination. Hence, under these experimental conditions, 4 g/L for AV 7 was found to be the optimum for efficient removal. At higher concentration of the catalyst (above 4 g/L), the decrease in efficiency is due to the light scattering by catalyst particles.[43] The increase of dye

concentration from 2 to 6 × 10^{-4} M the increases the photocatalytic degradation efficiency gradually upto 5× 10^{-4} M (88, 91, 95, 98 %) and then decreases (92 %). As the concentration of the dye increases, the path length of the photons entering the solution decreases. Thus, the photocatalytic degradation efficiency decreases at higher concentration of dye. While at low concentration the reverse effect is observed, thereby increasing photon absorption by the catalyst. The large amount of adsorbed dye may also have a competing effect on the adsorption of oxygen and OH^- onto the surface of catalyst.

We have examined the reusability of the Pr_6O_{11}-ZnO in the degradation AV 7 for four consecutive cycles under identical experimental conditions (Fig.11). The catalyst shows 99.4, 97, 95 and 95% efficiency in first, second, third and fourth cycles respectively. These results reveal that the synthesized Pr_6O_{11}-ZnO can be used several times in the degradation process. It is concluded that the synthesized Pr_6O_{11}-ZnO is a potential candidate for environmental remediation processes. We had taken XRD spectra of fresh and used Pr_6O_{11}-ZnO photocatalyst for four runs in AV 7 degradation, and they are given in Fig. S8. It was found that the crystal structure of used Pr_6O_{11}-ZnO photocatalyst did not change during the degradation, indicating the stability of photocatalyst.

3.3. Degradation Mechanism

Pr_6O_{11} had been used as a catalyst for the oxidation of Phenol, Carbon mono oxide and hydrogen.[44, 45] In case of dye removal, about 60% degradation was observed with Pr_6O_{11} while ZnO was able to degrade 68.2% dye in 90 minutes. But this coupled oxide Pr_6O_{11}-ZnO was able to degrade 98 % AV 7 dye in 90 minutes. This shows that the efficiency of ZnO is enhanced by the addition of Pr_6O_{11}. Pr_6O_{11} has been reported to have high electrical conductivity due to

electron hopping between the mixed metal ion valence states of the lattice.[19] In the catalyst, Pr (4+) can capture the electron and subsequently transfer to the adsorbed oxygen forming Pr (3+), so that electron-hole recombination is reduced. Higher electrical conductivity of Pr_6O_{11} also enhances the electron capture, which increases the photocatalytic activity of ZnO.

In the case of AV 7 dye, a dye-sensitized mechanism is also possible for the degradation. We carried out the degradation of AV 7 with 365 nm UV light ($I_{UV} = 1.381 \times 10^{-6}$ Einstein L^{-1} s^{-1}) under the same conditions used for natural sun light. It was found that AV 7 underwent 72.3% degradation with UV light, but under the same conditions 96.2% degradation occurred with solar light in 75 min. The higher efficiency in solar light indicates the presence of a dye-sensitized mechanism in addition to Pr_6O_{11}–ZnO sensitization. This occurs when more dye molecules are adsorbed on the semiconductor surface. Dark adsorption of dye on Pr_6O_{11}–ZnO (40.0 %) is higher when compared to ZnO (30.0%) and Pr_6O_{11} (17.5%). In this mechanism, the photoexcited electron is transferred from solar light-sensitized dye molecule to the conduction band of ZnO and this subsequently increases electron transfer to the adsorbed oxygen producing superoxide radicals. Dye molecules are degraded by the superoxide radicals produced by the dye sensitization mechanism (Equations 3-5). Further, to prove the dye-sensitized mechanism, we had also carried out an experiment for degradation of colorless 4-nitrophenol by Pr_6O_{11}–ZnO with UV and solar light. We found that degradation of 4-nitrophenol was more efficient in UV light (79.9%) than in solar light (40.4%) in 60 min under the same conditions, indicating the presence of only catalyst sensitized mechanism in the degradation of 4-nitrophenol.This confirms the presence of dye-sensitized mechanism for degradation of AV 7.

$$\text{dye} + Pr_6O_{11}\text{–ZnO} \longrightarrow \text{dye}^{+\bullet} Pr_6O_{11}\text{–ZnO} + e_{cb}^{-} \quad (3)$$

$$e_{cb}^{-} + O_2 \longrightarrow O_2^{\bullet -} \quad (4)$$

dye +• + O_2 / O_2•− ⟶ degradation products (5)

3.4. Contact angle measurements

Surface non-wettability or the hydrophobicity of the catalyst is revealed by water contact angle. If a surface has a contact angle with water that is greater than 90°, then the surface is classed as hydrophobic and if the contact angle is less than 90°, the surface is hydrophilic. Water contact angles were measured on glass slides coated with TEOS + Pr_6O_{11}, TEOS + ZnO and TEOS + Pr_6O_{11}-ZnO to analyze the hydrophobicity of the catalysts. Fig.12 shows the images of water drops on coated and uncoated glass slides. Water contact angle(WCA) of 39.7° on uncoated glass slide (CA1) shows the hydrophilicity and this WCA increases gradually on glass slides coated with TEOS + Pr_6O_{11} (62.8°), TEOS + ZnO (70.5°) and TEOS + Pr_6O_{11}-ZnO (101.1°). This shows that the surface coated with TEOS + Pr_6O_{11}-ZnO has more hydrophobic character. In TEOS, the OH groups get replaced by stable O-Si-O groups and these groups are modified by Pr_6O_{11}-ZnO to make the surface rougher, stable and non-wettable. That is why the contact angle increases above 90^o , exhibiting the hydrophobicity of the catalyst. This hydrophobicity increases the surface non-wettability, leading to a self cleaning property of the catalyst.

3.5. Conductivity Studies

A constant voltage of 1 V to 10 V was applied across the sample and DC conductivity was determined using the following equation (6). [46]

$$\sigma = \left(\frac{[(I \times L)]}{[(V \times A)]} \right) \quad \text{---------- (6)}$$

Where I- is the current, L- is the thickness of the sample, V-is the voltage and A-is the area of the sample. Fig.13A depicts the DC conductivity Vs Voltage response for the samples. It is observed that current increases linearly with increase in voltage for Pr_6O_{11}-ZnO sample. The increase of DC conductivity with increase in voltage shows the semi conducting nature of the crystal. Pr_6O_{11}-ZnO Quantum dots exihibit much higher conductivity than ZnO and Pr_6O_{11}.

Photoconductivity was measured by irradiating the sample with 100W halogen lamp.Fig. 13B represents the photoconductivity of the Pr_6O_{11}-ZnO. It is evident from fig. 13B that the photocurrent is higher than dark current. At 100 V/cm, the photocurrent of 5.0×10^{-5} mA is 1.35×10^{-5} mA higher than dark current (3.65×10^{-5} mA). This positive photoconductivity may be due to the increase of charge carriers on radiation. Materials exhibiting good DC and photoconductivity can be very much useful for soliton wave communication as well as solar cell applications.[47]

4. CONCLUSIONS

Pr_6O_{11}-ZnO semiconductor photocatalyst was synthesized by a facile hydrothermal method and characterized. XRD analysis reveals that the as synthesized product has face-centered cubic phase of Pr_6O_{11} and hexagonal wurtzite phase of ZnO. FE-SEM images of Pr_6O_{11}-ZnO shows the nanochain like structures and Pr_6O_{11} nanoparticles were homogeneously dispersed on the ZnO surface. HR-TEM images shows existence of quantum dots. The XPS analysis shows the presence of Zn, O and Pr elements and their oxidation states. Pr_6O_{11}-ZnO has increased absorption in the UV as well as visible region. Pr_6O_{11}-ZnO exhibit higher photocatalytic activity compared to pure ZnO and Pr_6O_{11} particles in the degradation of AV 7 dye. Pr_6O_{11}-ZnO is more advantageous in toxic dye degradation because of its reusability and

higher efficiency at the neutral pH 7 far exceeding of the single component systems. As TEOS + Pr_6O_{11}-ZnO is hydrophobic, it can be used as a self cleaning material for industrial applications. Pr_6O_{11}-ZnO exihibits good DC and Photoconductivity, which make the catalyst useful for soliton wave communication and solar cell applications.

Acknowledgements

Authors are thankful to the CSIR, New Delhi, for the financial support through research Grant no. 21 (0799)/10/EMR-II. One of the authors S. Balachandran acknowledges UGC Networking Resource Centre, University of Hyderabad, for providing the characterization facility and is thankful to Dr. Tushar Jana, School of Chemistry, University of hyderabad, for the lab facility**.** Authors are also grateful to Dr. P.V. Satyam, Institute of Physics, Bhubaneswar for HR-TEM facility.

CAPTIONS FOR FIGURES AND SCHEME

Fig. 1 Thermal analysis of (a) Prepared Zinc Oxalate and (b) Pr $(OH)_3$ –Zinc Oxalate

Fig. 2 XRD patterns of (a) Prepared ZnO, (b) $Pr(OH)_3$-ZnO and (c) 9wt% Pr_6O_{11}−ZnO

Fig. 3 FE-SEM images of 9wt% Pr_6O_{11}−ZnO at different magnification (a) 100K, (b) 50K, (c) 75K and (d) 150K.

Fig. 4 FE-SEM elemental colour mapping image of (a) Pr_6O_{11}−ZnO, (b) Zn, (c) O and (d) Pr.

Fig. 5 HR-TEM images of 9wt% Pr_6O_{11}−ZnO (a, c) Particle at different location, (b, d) Lattice fringes, (e) SAED pattern and (f) average particle size

Fig. 6 XPS analysis of 9wt% Pr_6O_{11}−ZnO (a) Survey spectrum, (b)O 1s , (c) Zn 2p and (d) Pr 3d

Fig. 7 Diffuse reflectance spectra of (a) Prepared ZnO and (b) 9wt% Pr_6O_{11}−ZnO

Fig. 8 Photoluminescence spectra of (a) Prepared ZnO and (b) 9wt% Pr_6O_{11}−ZnO

Fig. 9 N_2 adsorption−desorption isotherms of (a) 9wt% Pr_6O_{11}−ZnO and (b) their pore size distribution.

Fig. 10 Photodegradability of AV 7 with different catalysts: AV 7 dye concentration = 5×10^{-4} M, catalyst suspended = 3 g L^{-1}, pH = 7, airflow rate = 8.1 mL s^{-1}, I_{solar} = 1250×100Lux ±100 and irradiation time 90 min. (a) Dye + Solar, (b) Dye + Pr_6O_{11}-ZnO + Dark, (c) Dye + Pr_6O_{11} + Solar, (d) Dye + ZnO + Solar, (e) Dye + Pr_6O_{11}-ZnO + Solar

Fig. 11 Reusability of Pr_6O_{11}-ZnO with AV 7 dye degradation

Fig. 12 Water contact angle measurements

Fig. 13 (A) DC conductivity (S/cm) Vs Voltage (V) curve, (B) Photoconductivity of Pr_6O_{11}-ZnO. Applied electric field (V/cm) vs. electric current (mA). (a) dark and (b) on irradiation with 100 W halogen lamp.

Scheme 1. Preparation of heterostructured Pr_6O_{11}-ZnO

Scheme 2. Degradation Mechanism

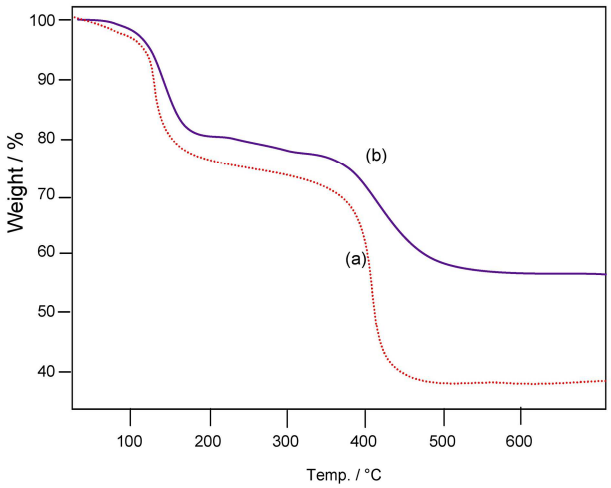

Fig. 1

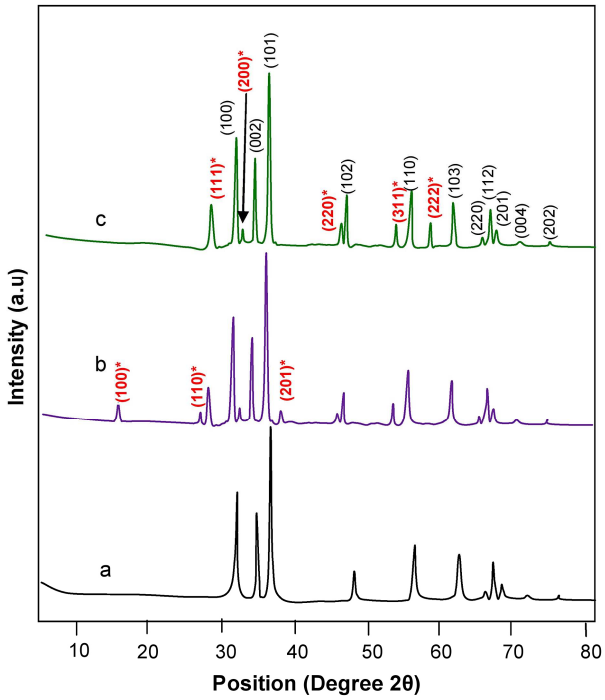

Fig. 2

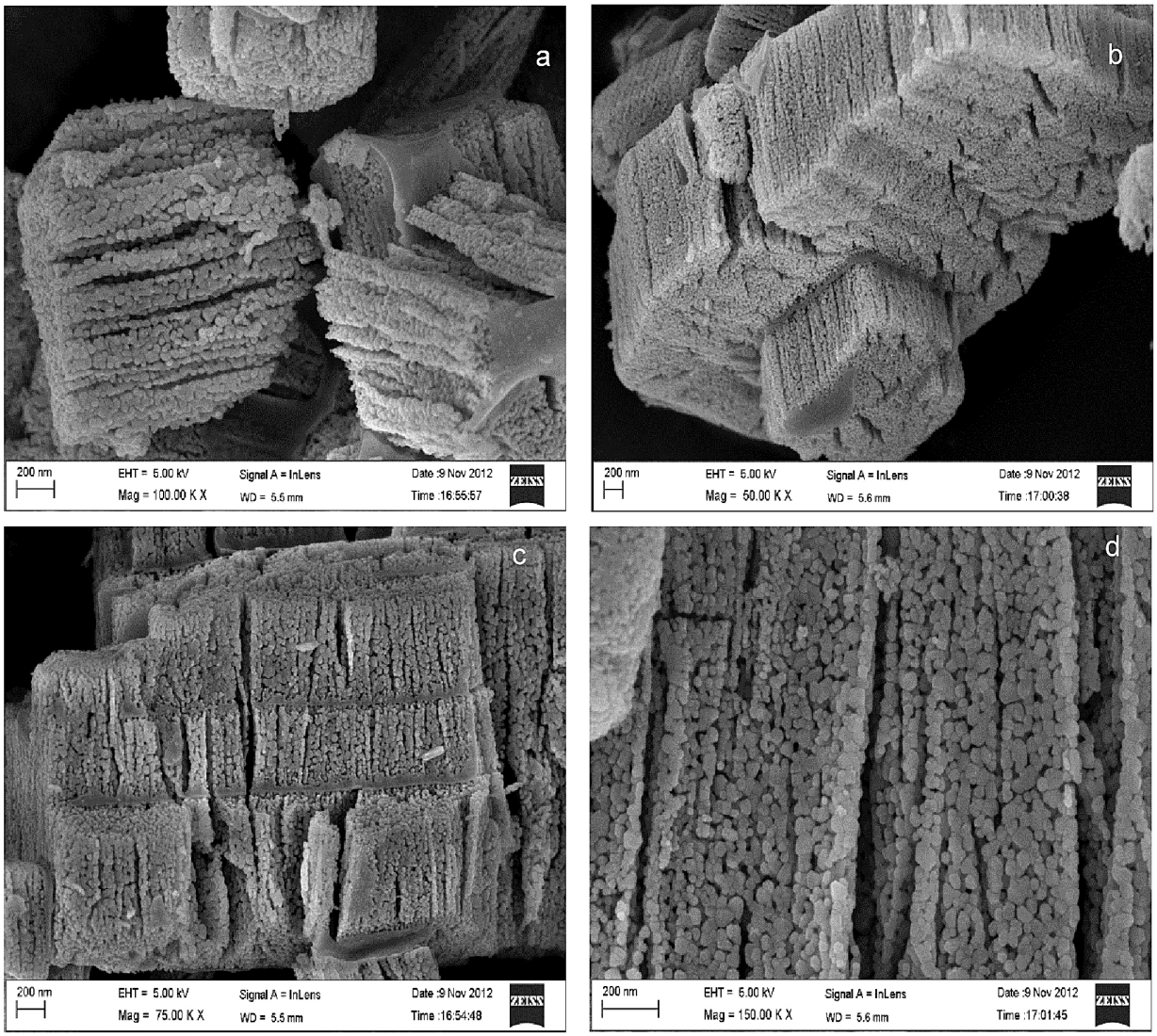

Fig. 3

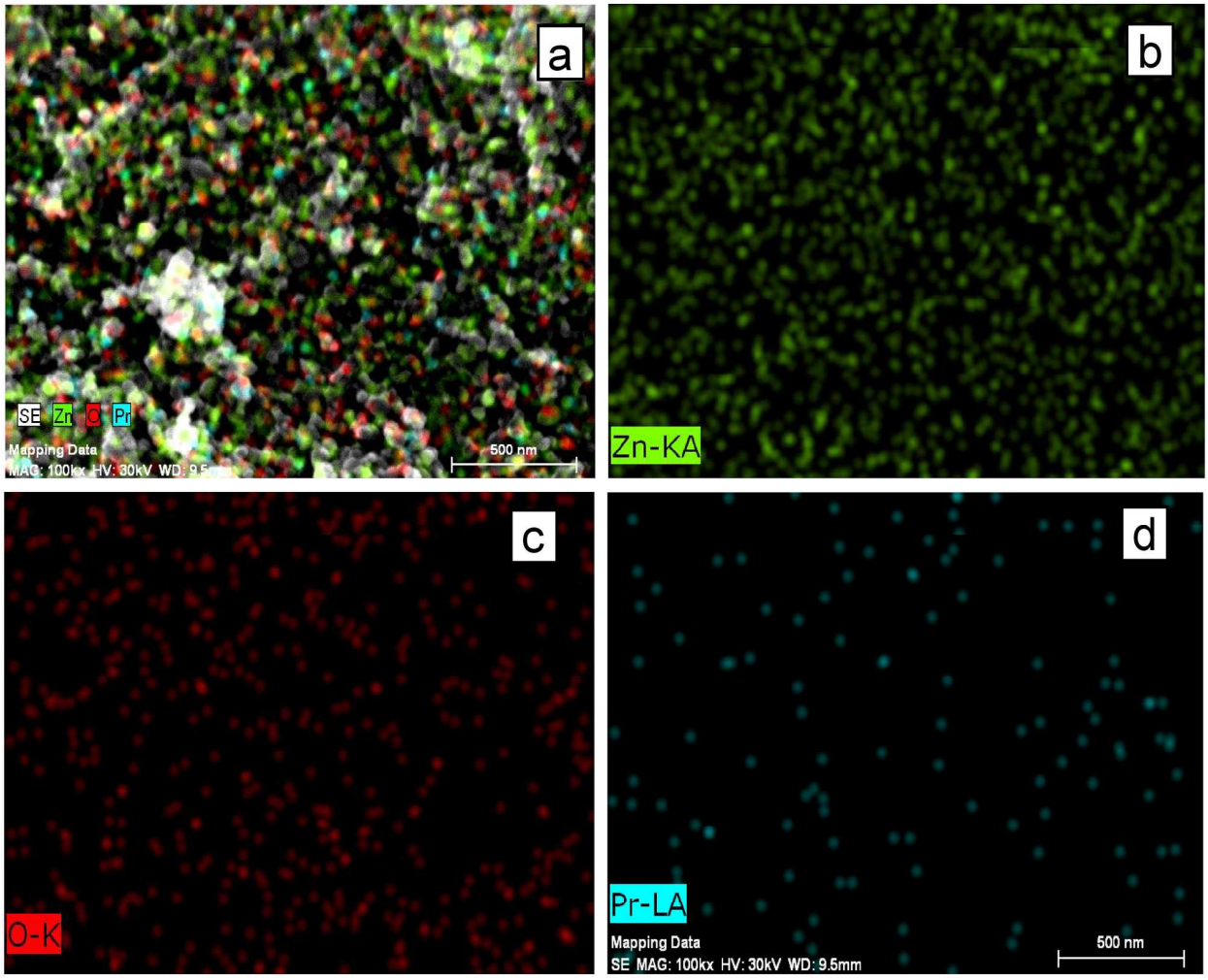

Fig. 4

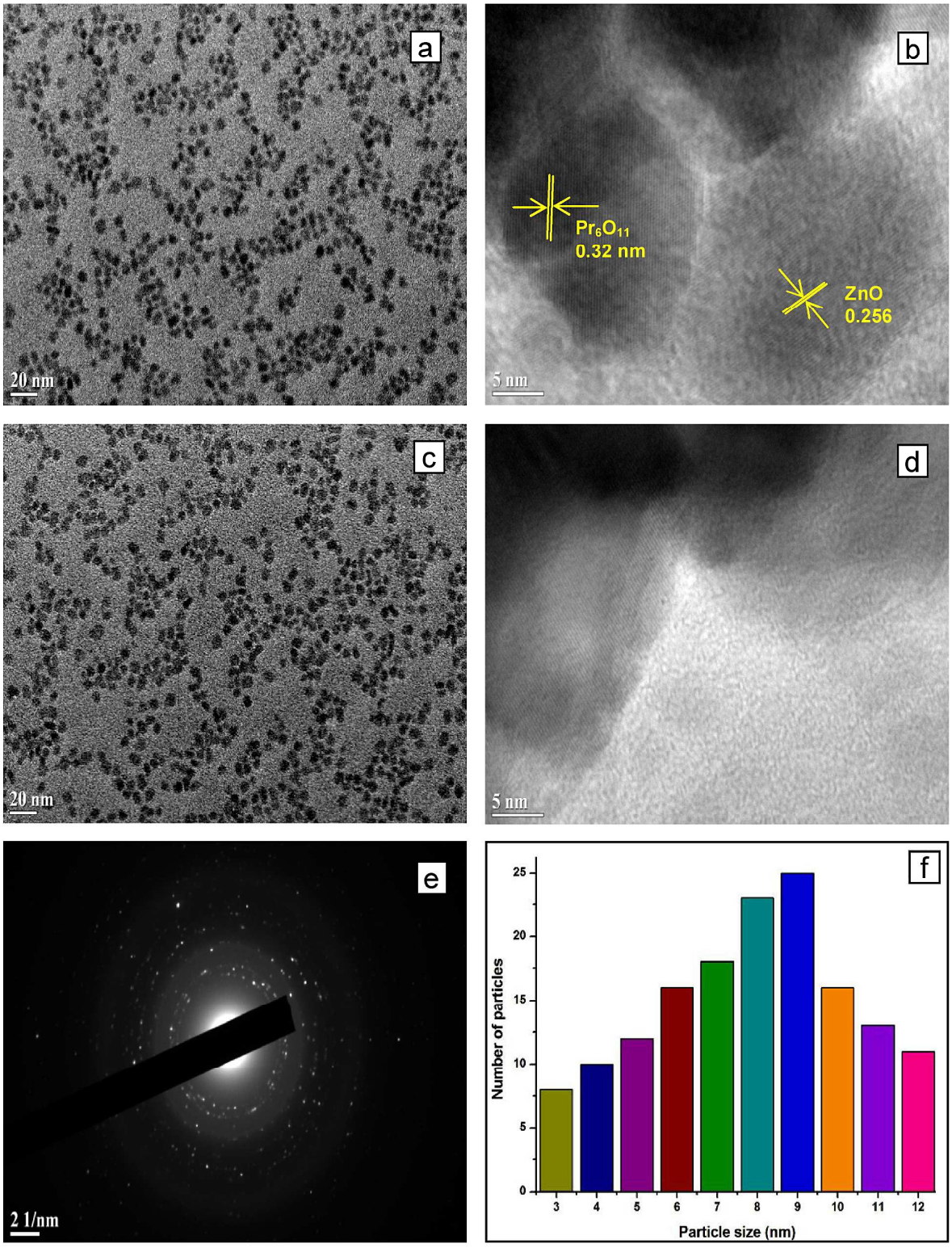

Fig. 5

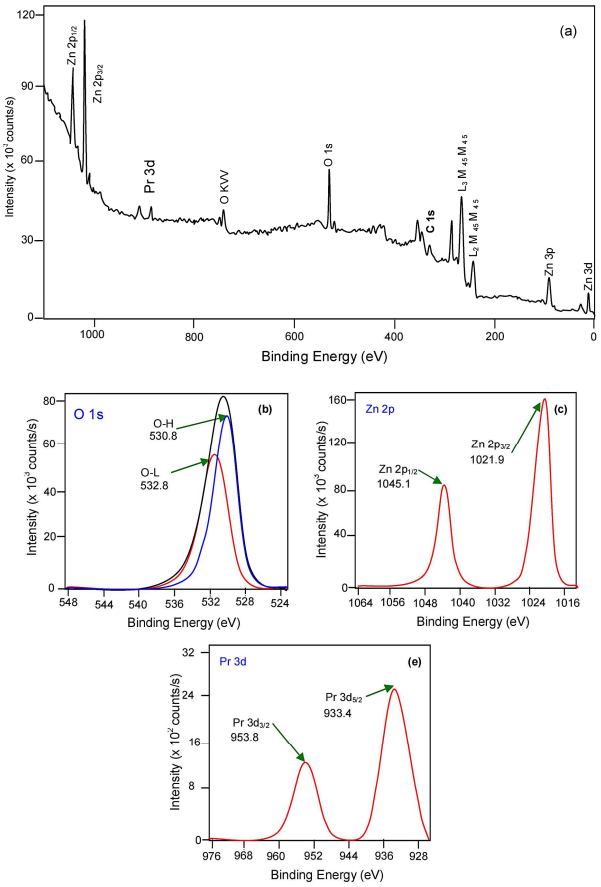

Fig. 6

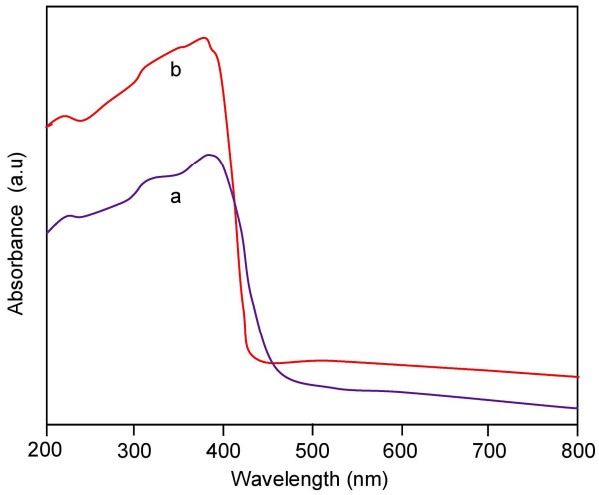

Fig. 7

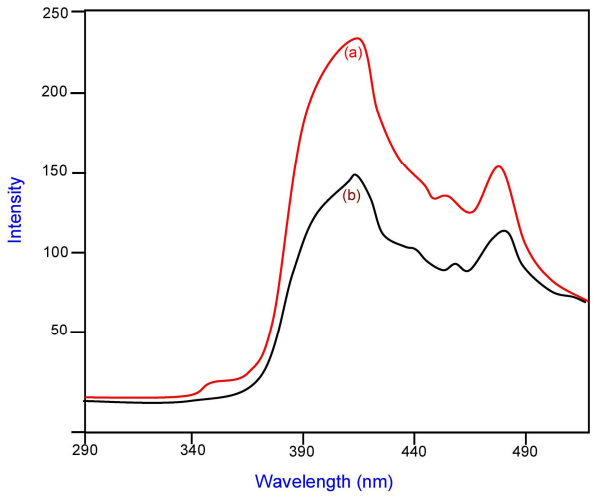

Fig. 8

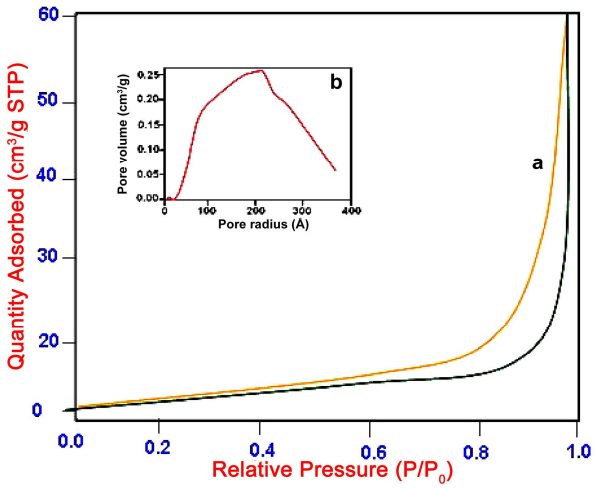

Fig. 9

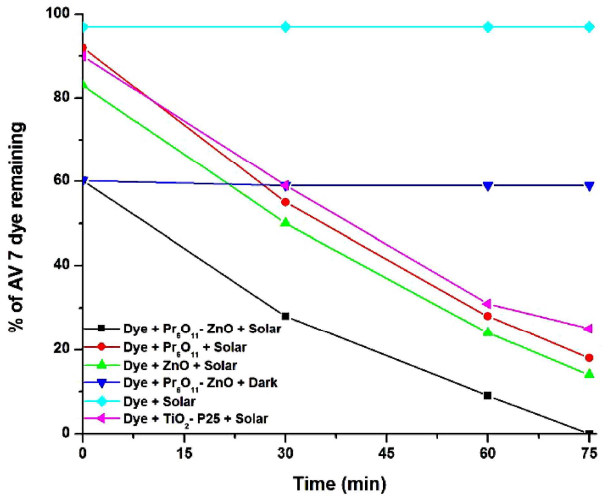

Fig. 10

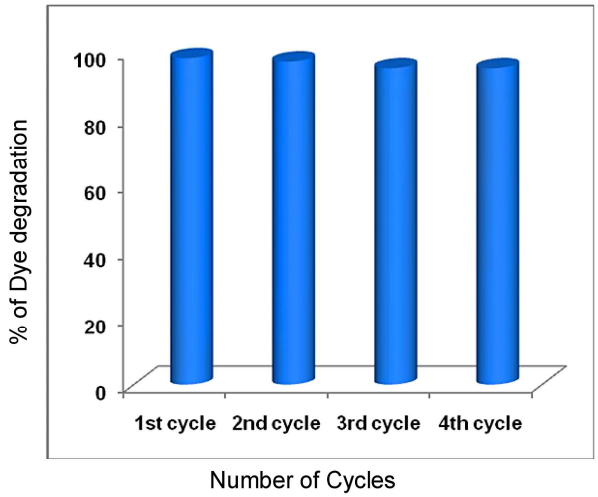

Fig. 11

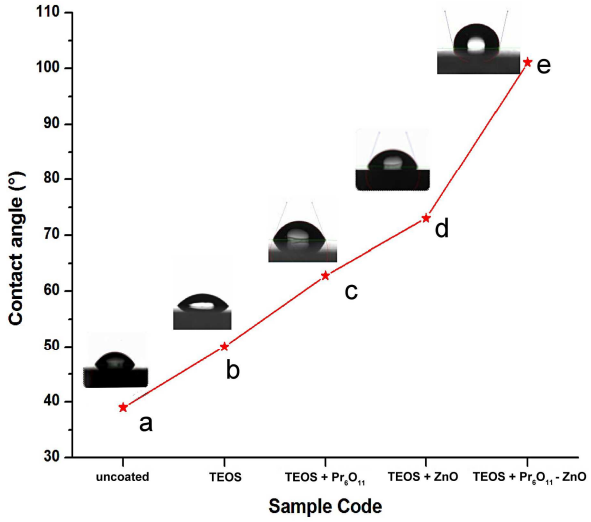

Fig. 12

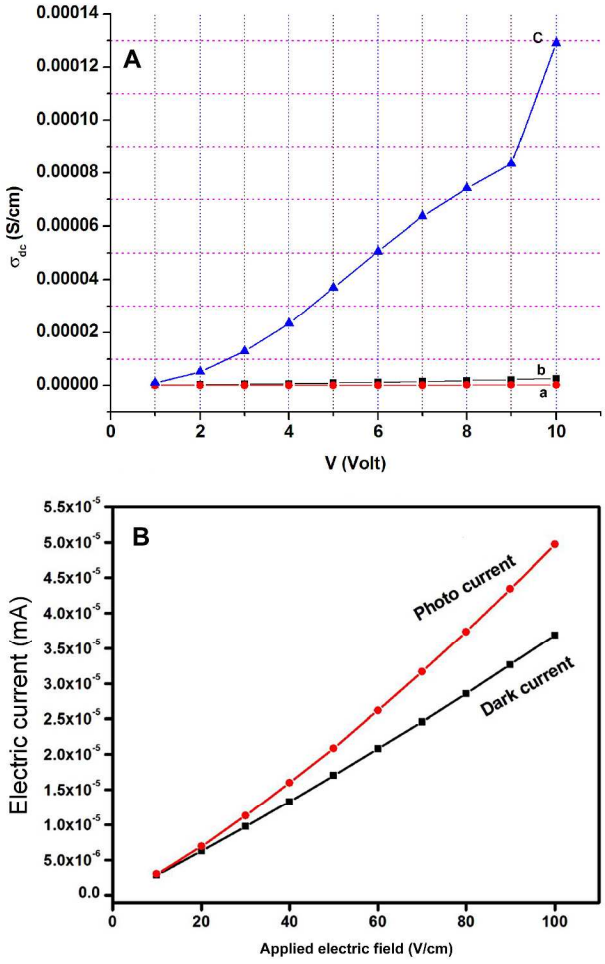

Fig. 13

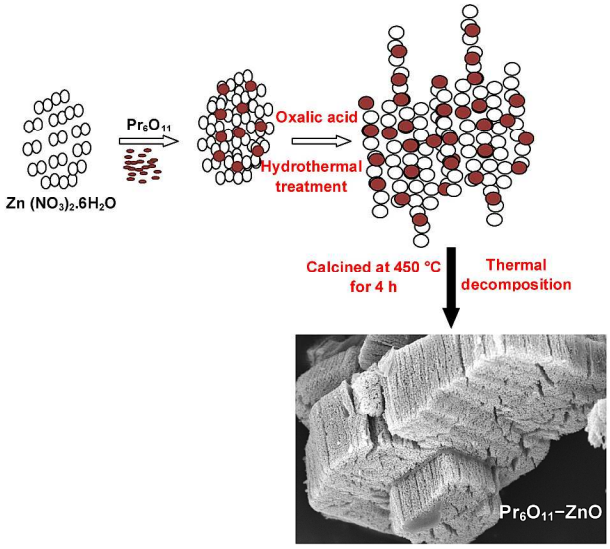

Scheme 1

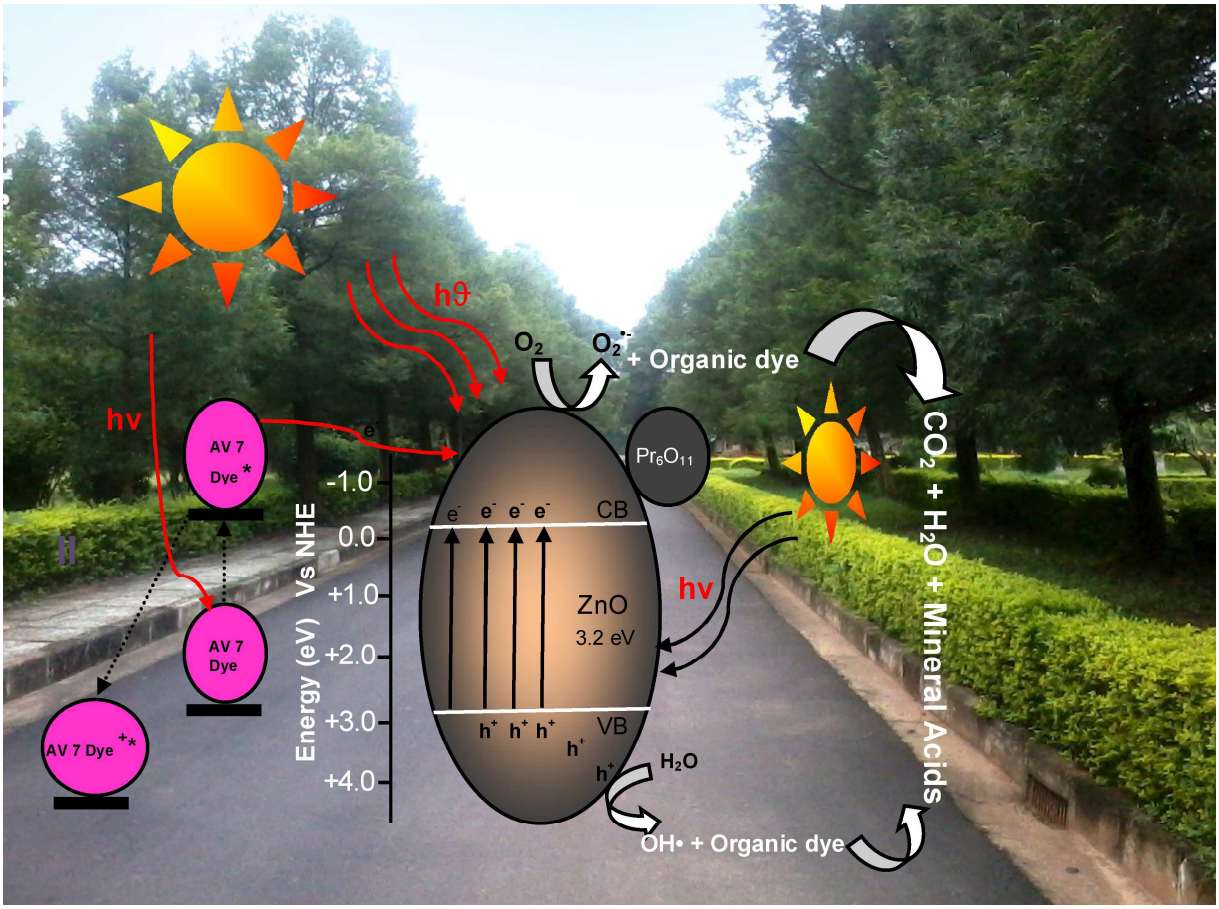

Scheme 2

Graphical abstract

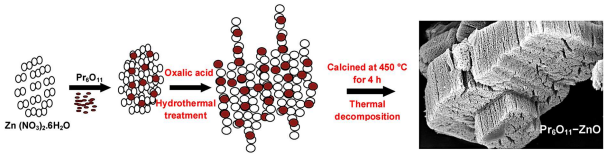

A simple hydrothermal process has been used for the synthesis of Pr_6O_{11}-ZnO. This heterostructured photocatalyst shows higher photocatalytic activity for the degradation of AV 7 dyes, under solar light than pure ZnO, Pr_6O_{11}, and commercial Degussa P25 due to the low recombination rates of photoinduced electron-hole pairs.